Cloud condensation nuclei (CCN) and ice nuclei (IN) abilities of Al_2O_3 and Fe_2O_3 using MRI dynamic cloud chamber and CFDC-type IN counter

Tzu-Hsien KUO[1], Masataka MURAKAMI[1,2]
Takuya TAJIRI[1], and Narihiro ORIKASA[1]
[1]MRI; [2]ISEE, Nagoya U.

2017/02/17@極地研

Outline

- General information of two metal oxide
  - Reviewed articles in atmospheric composition
- Reviewed articles in cloud chamber and CFDC experiments
- MRI experiments during 2016/10/17-2017/01/16
  - Particle size distribution
  - CCN abilities (κ-value)
  - IN abilities (dynamic cloud chamber/CFDC type IN counter)
- Discussion
- Conclusion and ongoing work

General information of two metal oxide

- Metal oxide sources in the atmosphere
  - Natural– volcano, soil, biomass burning
  - Anthropogenic- engineered, fuel, industrial pollution, firework, aircraft emission, hygroscopic flare

Aluminium oxide observed in the atmosphere

Aluminium accounts for 8.3% of Earth crust;
Corundum is the most common naturally occurring crystalline form of aluminium oxide.
Industrial proposes

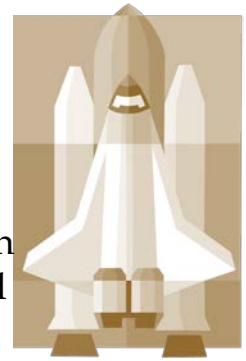

Space shuttle exhausted air at 2-7 km high with 98.9% aluminum oxide in 0.3 μm diameter and below. (Cofer III et al., 1991)

Roadside: 23.1% in aluminum oxide (Sanderson et al.,2016)

In Abidjan- a rural (Pasteur), an urban (Cocody), an industrial (Vridi) sites, particles are mostly smaller than 2.5 μm, aluminum, iron, calcium account for 56-79 μg/mg, 34-54 μg/mg and 31-37 μg/mg. (Kouassi et al., 2010)

From wikipedia

Linak et al., (2007):Fly-ash includes Al, Ca, Ti,Mg, and iron oxide is below 2.5 μm

Component	Bituminous	Subbituminous	Lignite
Al_2O_3	5-35	20-30	20-25

Iron oxide observed in the atmosphere

Iron accounts for 4.5% of Earth crust;
Industrial proposes

In urban background, iron oxide distributes in 25-116 nm (Belosi et al., 2013)

Iron oxide distributes 200-2400 nm in Tsukuba. (Adachi et al., 2016)

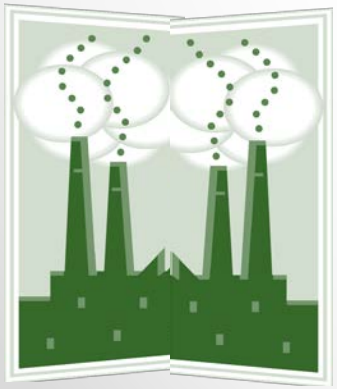

Around iron and steel manufacturing facilities, iron oxide distributes 5-10 μm or less 5 μm. (Machemer, 2004)

Roadside: 52.6% iron in PM_{18}, iron oxide's median diameter 27 and 37nm. (Sanderson et al.,2016)

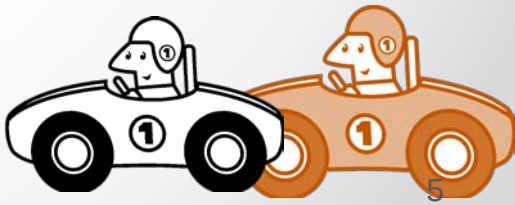

Anthropogenic forcing

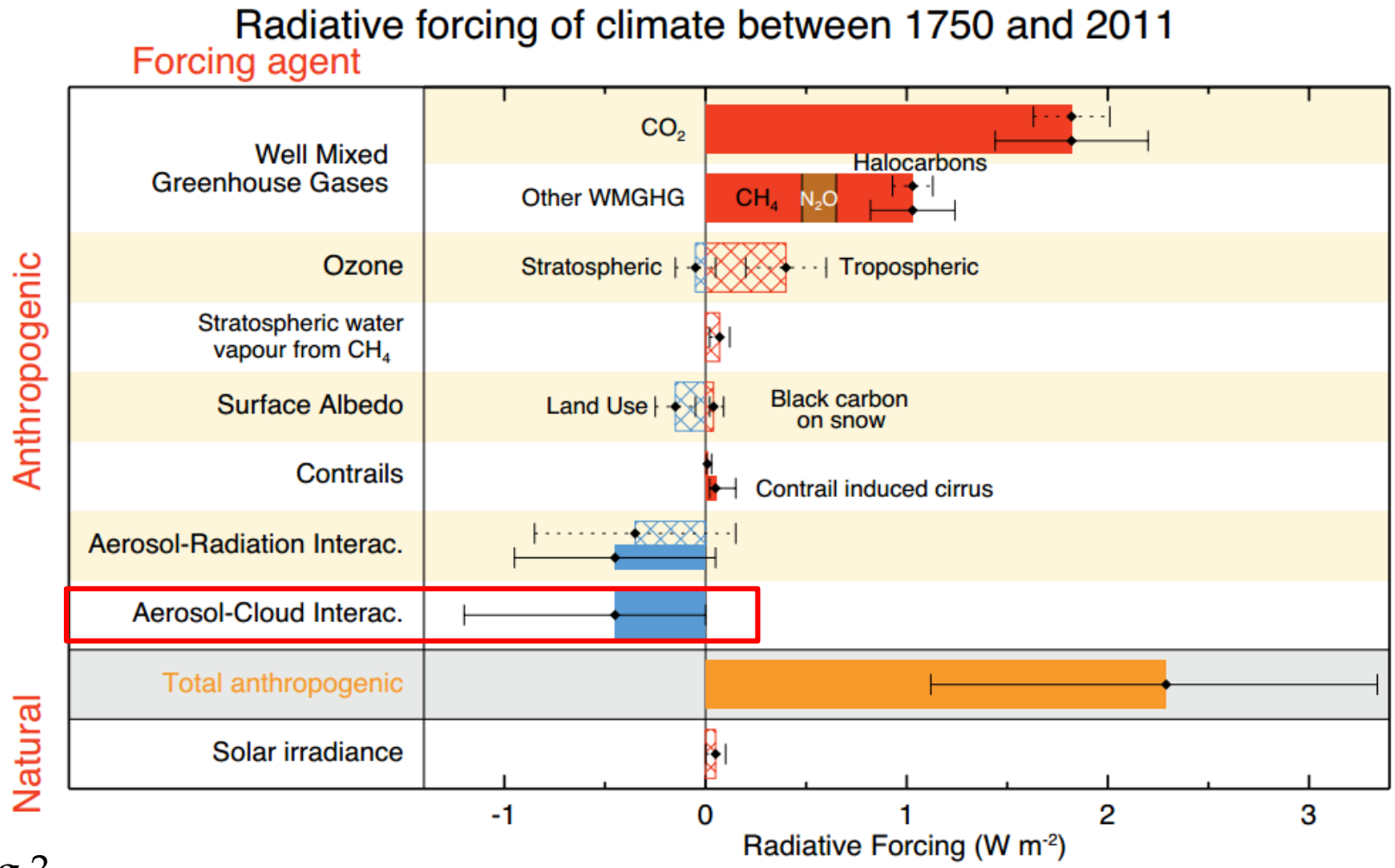

Fig 3. Bar chart for RF (hatched) and ERF (solid) for the period 1750–2011, where the total ERF is derived from Figure 8.16. Uncertainties (5 to 95% confidence range) are given for RF (dotted lines) and ERF (solid lines).

(IPCC, AR5)

Aerosol—cloud—climate interaction

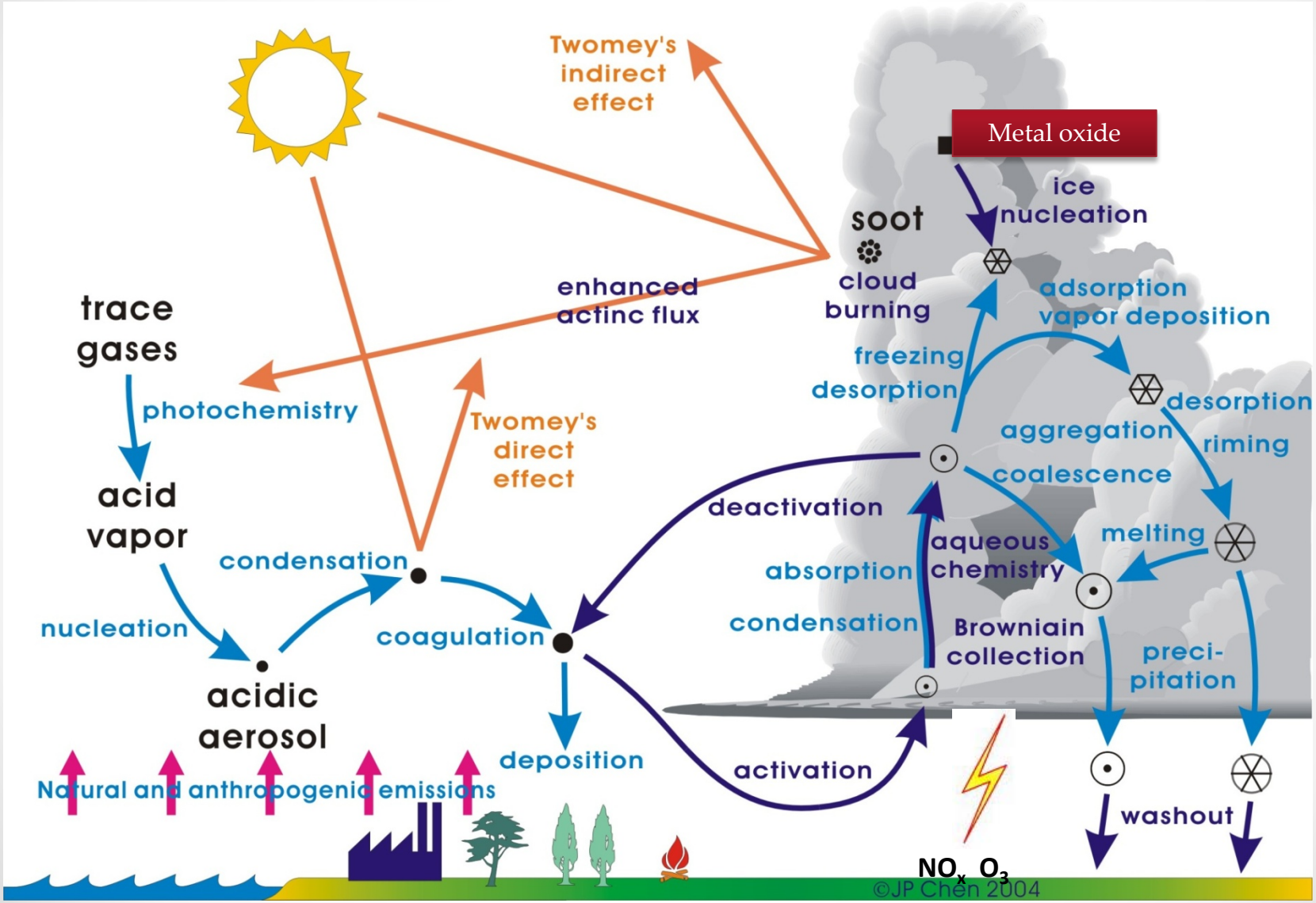

Fig 4. Aerosol-cloud-climate interaction (J.-P. Chen 2004)

Ice nucleation

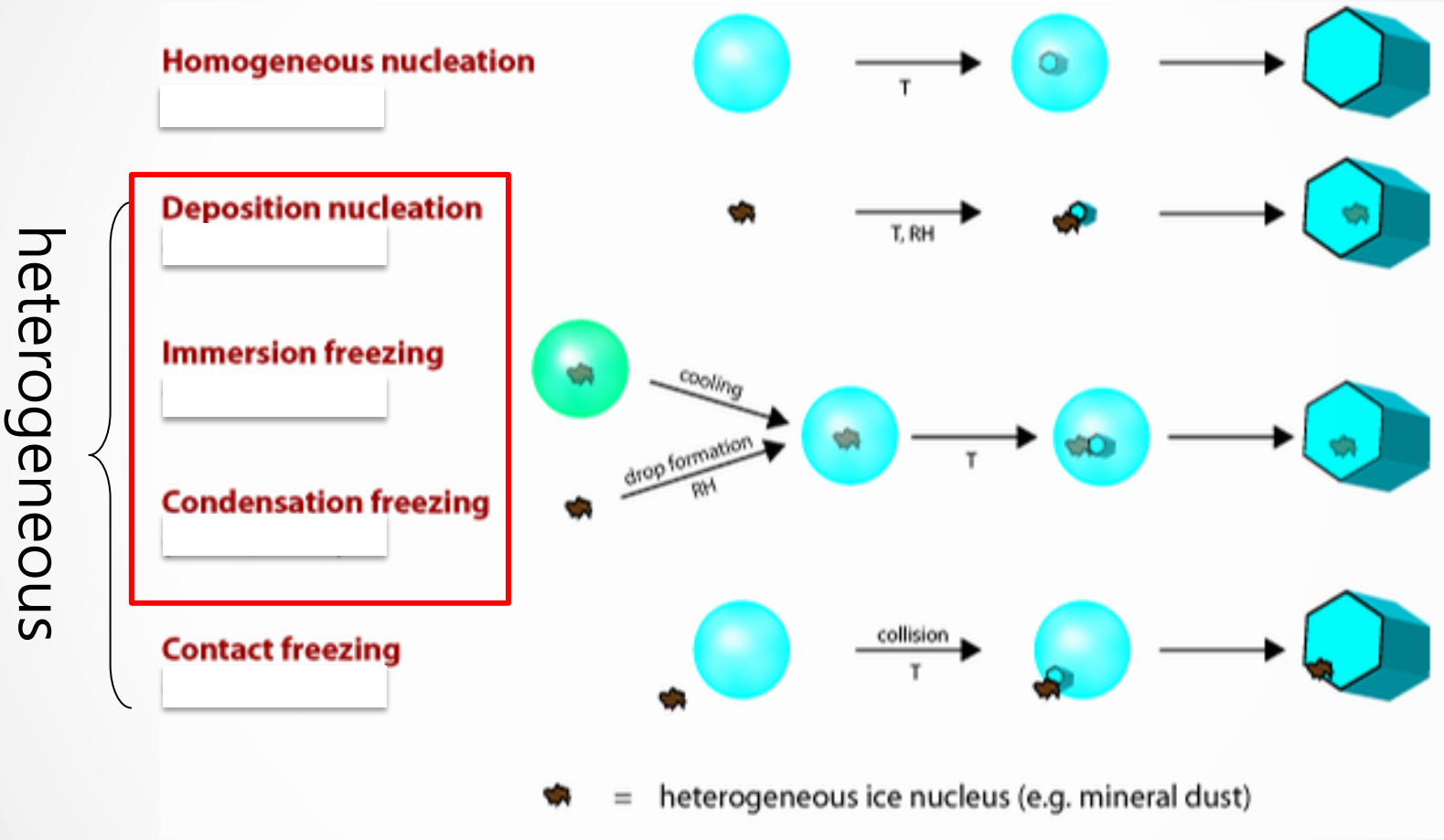

Fig 5. Modes of ice formation in clouds (from ETH Zürich)

Ice nucleation active surface site (INAS) densities

- INAS density (*ns*) based on geometric aerosol size is a method to parameterize surface area-scaled immersion freezing activities (Connolly et al., 2009; Niemand et al., 2012)

- postulates that ice crystal formation observed in experiments is a solely function of temperature (and ice saturation)
- activated ice crystals (*Nice*) and CN was measured simultaneously during the expansion experiments, the activated fraction of aerosol particles as ice nuclei (*fIN* = *Nice*/*Ncn*) was obtained
- dividing the activated fraction by the volume equivalent surface area of an individual particle (*Sve*) measured in advance for each experiment
- on the assumption of a uniform distribution of ice nucleation sites and their size-independency over a given total aerosol surface area (*Sve* • *Ncn*).

$$n_s(T, S_i) = -1/A_{aer} \cdot \ln(1 - f_{IN}(T, S_i)) \approx f_{IN}(T, S_i)/A_{aer}$$

Reviewed articles – AIDA chamber

- Hiranuma et al. (2014) used AIDA chamber, shown with **immersion nucleation,** tested surface irregularities of Fe_2O_3
  - The immersion mode ice nucleation efficiency of **milled** Fe_2O_3 particles is almost an order of magnitude higher at −35.2 ℃ < T <−33.5 ℃ (RH_i = 125%) than that of the **cubic** Fe_2O_3 particles, indicating a substantial effect of **morphological irregularities** on immersion mode freezing

$$n^{c}_{s,geo}(T) = 1.072\times10^{8} + 1.777\times10^{-6} \times \exp(-0.969\times T),$$

$$n^{m}_{s,geo}(T) = 2.523\times10^{9} + 2.605\times10^{-4} \times \exp(-0.889\times T),$$

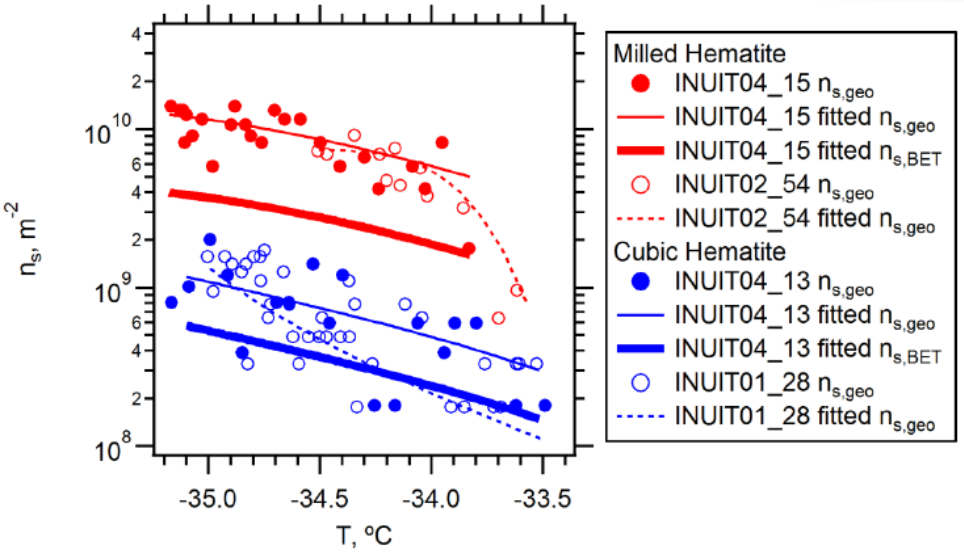

Fig 8. Results in INAS form

Reviewed articles – AIDA chamber

- Saunders et al. (2010) used AIDA chamber, observed **deposition** nucleation of Fe_2O_3 at RH_i ranging from 105% to 140% for temperatures below -53℃.
  - Approximately 10% of amorphous Fe_2O_3 particles (modal diameter = 30 nm) generated at RH_i = 140% with an initial chamber temperature of -91℃.
- Conditions studied in the chamber which correspond to cirrus cloud formation in the upper troposphere.

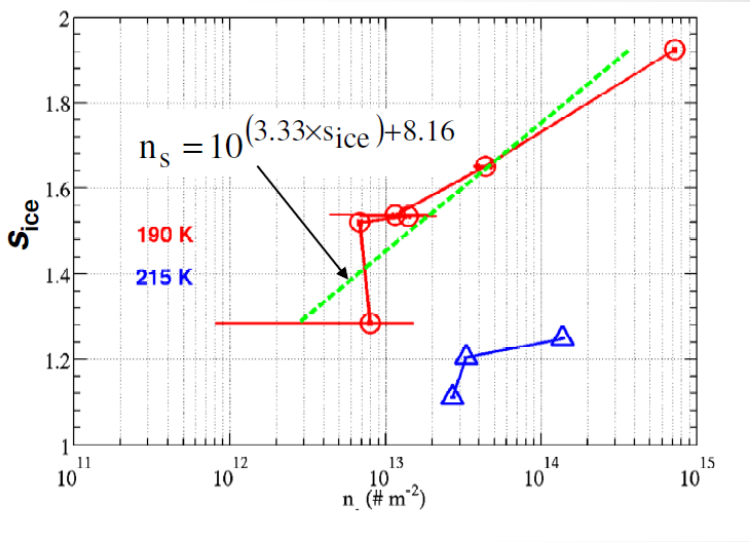

Fig 7. calculated number of active sites per unit area of material that become active at the given sice for the iron oxide aerosol experiments as indicated.

[ns (-83℃)=$10^{(3.33 \times Sice)+8.16}$]

Reviewed articles – CFDC

Yakobi-Hancock et al.(2013) using a CFDC at −40.0±0.3℃ and particles size-selected at 200 nm.

Table 1. Tested substances in order of increasing critical RH_i for deposition activation of 0.1 % of 200 nm particles at −40 °C. The electrical conductivity (µS) of the suspensions is indicated in parentheses for MDD, ATD, orthoclase, and TiO_2 after the sample names.

Sample	Critical RH_i (%)	Category	Source
PbI_2	122.8 ± 2.0	Anthropogenic	Sigma-Aldrich, 99 %
MDD unwashed (70 µS)	125.4 ± 1.8	Mineral dust	Peters et al. (2008)
MDD (50µS)	126.3 ± 3.4	Mineral dust	Peters et al. (2008)
Orthoclase (K-feldspar) (18 µS)	127.1 ± 6.3	Feldspar mineral	Department of Earth Sciences, University of Toronto
ATD (30 µS)	129.5 ± 5.1	Mineral dust	Powder Technology Inc., 0–5 µm
ATD unwashed (89 µS)	132.9 ± 0.5	Mineral dust	Powder Technology Inc., 0–5 µm
Orthoclase (K-feldspar) unwashed (50 µS)	135.0 ± 3.6	Feldspar mineral	Department of Earth Sciences, University of Toronto
Plagioclase (Na/Ca-feldspar)	136.2 ± 1.3	Feldspar mineral	Department of Earth Sciences, University of Toronto
Kaolinite	136.4 ± 1.9	Clay mineral	
Montmorillonite	139.3 ± 1.0	Clay mineral	
Illite	142.5 ± 2.3	Clay mineral	
Pyrite (FeS)	142.9 ± 0.8	Metal sulfide	
Corundum (Al_2O_3)	143.2 ± 3.2	Metal oxide	Sigma-Aldrich, ≥98 %
Calcite ($CaCO_3$)	144.3 ± 0.9	Metal carbonate	Department of Earth Sciences, University of Toronto
Magnetite (Fe_3O_4)	144.4 ± 2.2	Metal oxide	Sigma-Aldrich, < 5 µm, 95 %
Quartz (SiO_2)	144.7 ± 1.5	Metal oxide	Alfa Aesar, 99.9 %
Gypsum ($CaSO_4 2H_2O$)	144.8 ± 1.2	Metal sulfate	Sigma-Aldrich, ≥99 %
Galena (PbS)	145.0 ± 1.0	Metal sulfide	Sigma-Aldrich, 99.9 % trace metal basis
Anglesite ($PbSO_4$)	145.1 ± 1.3	Metal sulfate	Sigma-Aldrich, 98 %
Zn	145.4 ± 0.6	Pure metal	Atlantic Equipment Engineers, 99.8 %
Massicot (PbO)	145.5 ± 1.3	Metal oxide	Sigma-Aldrich, ≥99.0 %
Calcite ($CaCO_3$)	145.8 ± 1.4	Metal carbonate	Sigma-Aldrich, ≥99.0 %
Rutile (TiO_2) unwashed (10.8 µS)	146.3 ± 1.0	Metal oxide	Sigma-Aldrich, 99–100.5 %
Bunsenite (NiO)	146.5 ± 0.8	Metal oxide	Sigma-Aldrich, 99 %
Cerussite ($PbCO_3$)	146.7 ± 0.6	Metal carbonate	Sigma-Aldrich, ACS reagent grade
Rutile (TiO_2) (1.4 µS)	147.4 ± 0.4	Metal oxide	Sigma-Aldrich, 99–100.5 %
ZnS	147.7 ± 1.5	Metal sulfide	Sigma-Aldrich, ≥97.0 %
Zincite (ZnO)	148.6 ± 0.2	Metal oxide	Sigma-Aldrich, ≥99.0 %
Hematite (Fe_2O_3)	148.8 ± 1.0	Metal oxide	Sigma-Aldrich, < 5 µm, 99+ %

0.1% of the total number of injected aerosol particles had nucleated ice (i.e. formed 5 µm crystals)

Summary of reviewed articles

Table 2. Summary of reviewed articles

	Nucleation mode	Particle size	Results
Hiranuma et al. (2014)	Immersion (AIDA chamber)	modal diameter = 1 μm	**milled** Fe_2O_3 INAS~1E10 at −35.2 ℃ < T <−33.5 ℃ (RH_i = 125%) (larger particle)
Saunders et al. (2010)	Deposition (AIDA chamber)	modal diameter = 30 nm	Fe_2O_3 at RH_i ranging from 105% to 140% for temperatures below -53 ℃. (Upper layer)
Yakobi-Hancock et al. (2013)	Deposition (CFDC)	200 nm	-40℃, 1%, RHi=143.2% (Al_2O_3) RHi=148.8% (Fe_2O_3)
Archuleta et al. (2005)	Deposition (CFDC)	50,100,200 nm	200nm, 1%, RH_i ~140% -45 (Al_2O_3) -60 ℃ (Fe_2O_3)

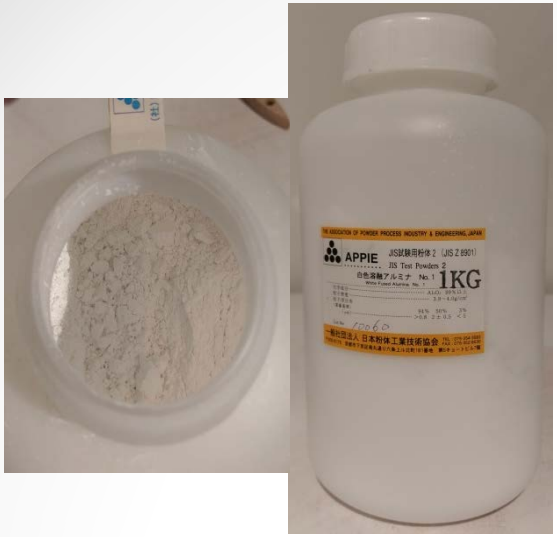

Table 4. Material information

Aerosol (source)	Purity wt%	Density (g cm^{-3})	Other content	Average surface (m^2)
Al_2O_3 (APPIE)	99% up	3.9	unknown	1.61E-12 (11/17)
$Fe_2O_{3\#1}$ (TETSUGEN)	99.24%	5.2	H_2O 0.1%, Cl 0.073%, SO_4 0.04%	8.04E-13 (2/13)
$Fe_2O_{3\#2}$ (TETSUGEN)	99.05%	5.2	H_2O 0.06%, Cl 0.04%, SO_4 0.02%	3.85E-13 (11/16)

Size distribution in the exp.

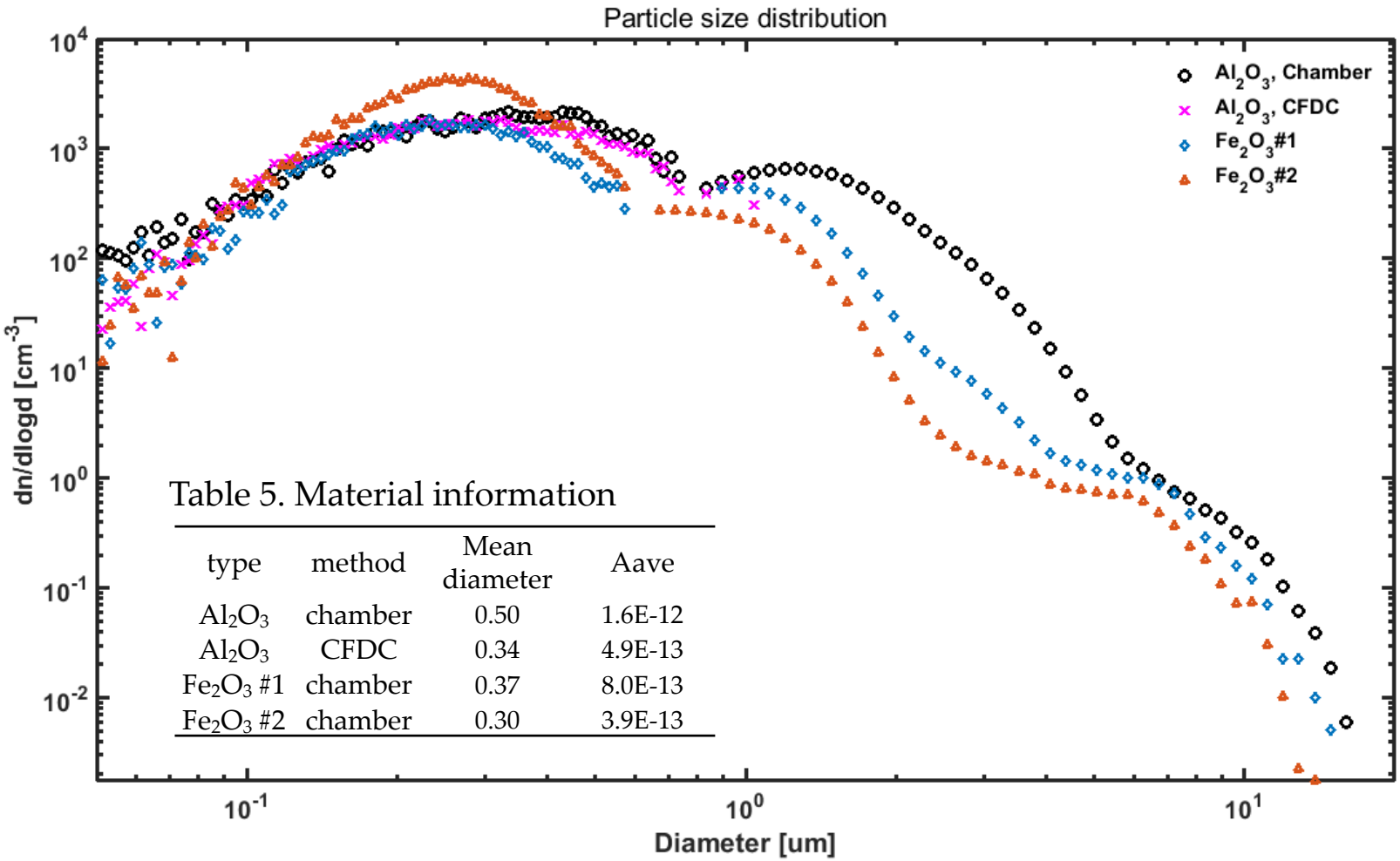

Table 5. Material information

type	method	Mean diameter	Aave
Al_2O_3	chamber	0.50	1.6E-12
Al_2O_3	CFDC	0.34	4.9E-13
Fe_2O_3 #1	chamber	0.37	8.0E-13
Fe_2O_3 #2	chamber	0.30	3.9E-13

Fig 10. Particle size distribution

Hygroscopicity measurement system

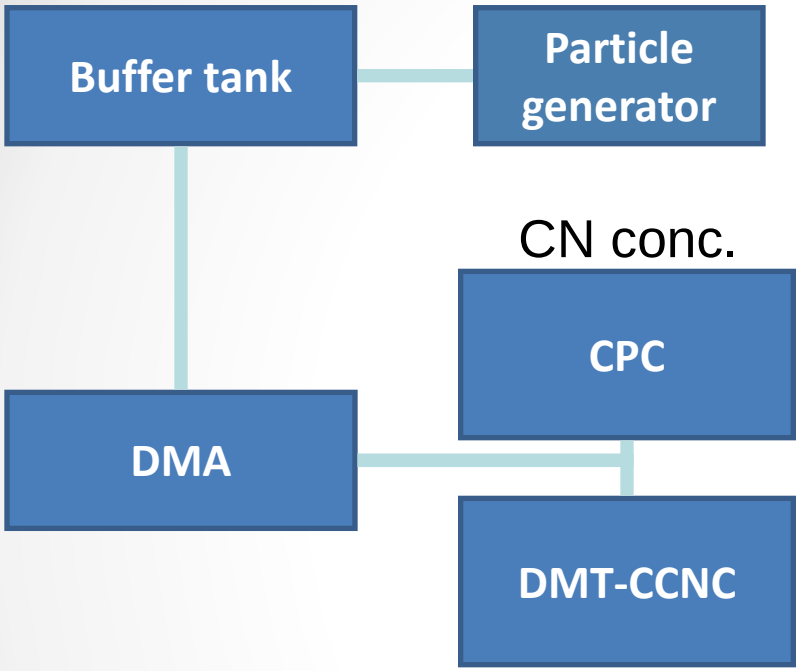

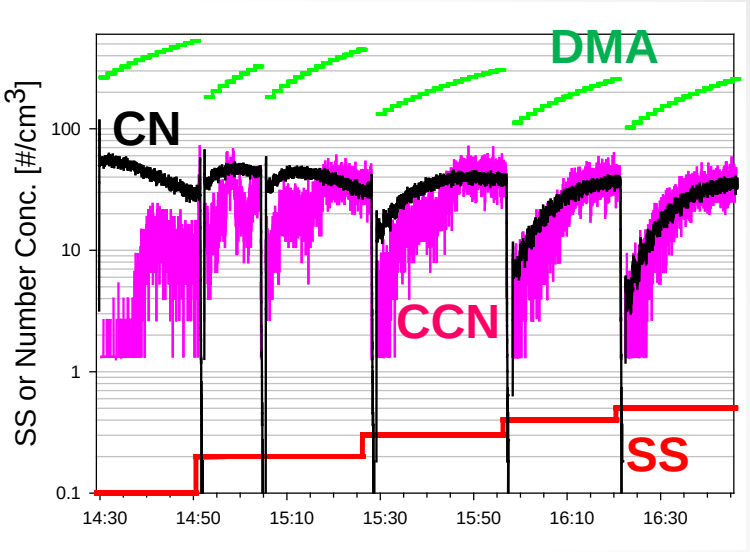

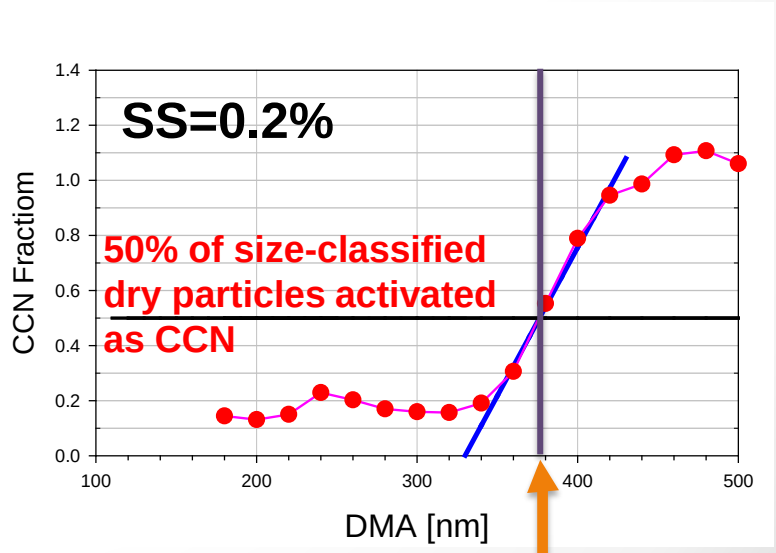

Activated Fraction(AF)

AF = CCN/CN

Critical Dry diameter: AF = 0.5

Kappa

The results indicated that the hygroscopicity (κ-value) were around 0.01, which are comparable to that of surrogates of mineral dust particles, and less than the average κ-value of atmospheric aerosols.

Fig.12 Kappa in experiments.

Aerosol and Cloud particles measurements

Aerosol Particles

CCN Counter
(CCN-200, DMT)

IN Counter
(MRI)

OPC
(KC-01E, RION)

SMPS
(MODEL3936, TSI)

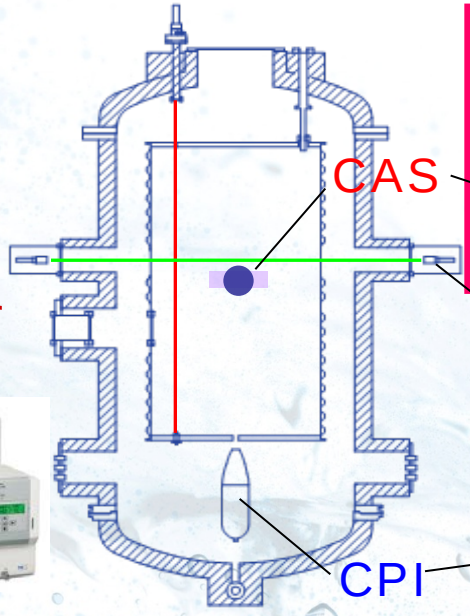

Cloud Particles

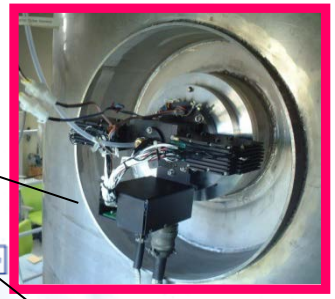

Laser sensor

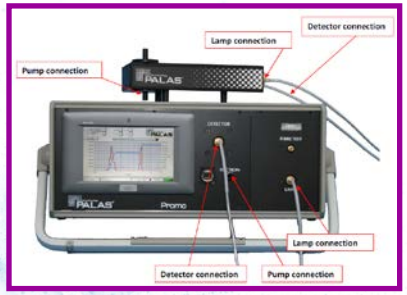

Welas OPC

Device specifications

Size range:
10nm～(aerosol)～1μm
～(drop/Ice)～100μm
Data: Aerosol size spectra,
CCN activity spectra
Cloud particle size distribution

Operational Ranges

Pressure: 1000 ～ 30hPa
Wall Temperature: +30 ～ -100 ℃
Ascent Rate: 0 ～ 30m/s

data：Onset, Time evolution of size distribution and concentration, Particle shape and Habit image and Depolarization ratio

MRI cloud chamber facility System diagram

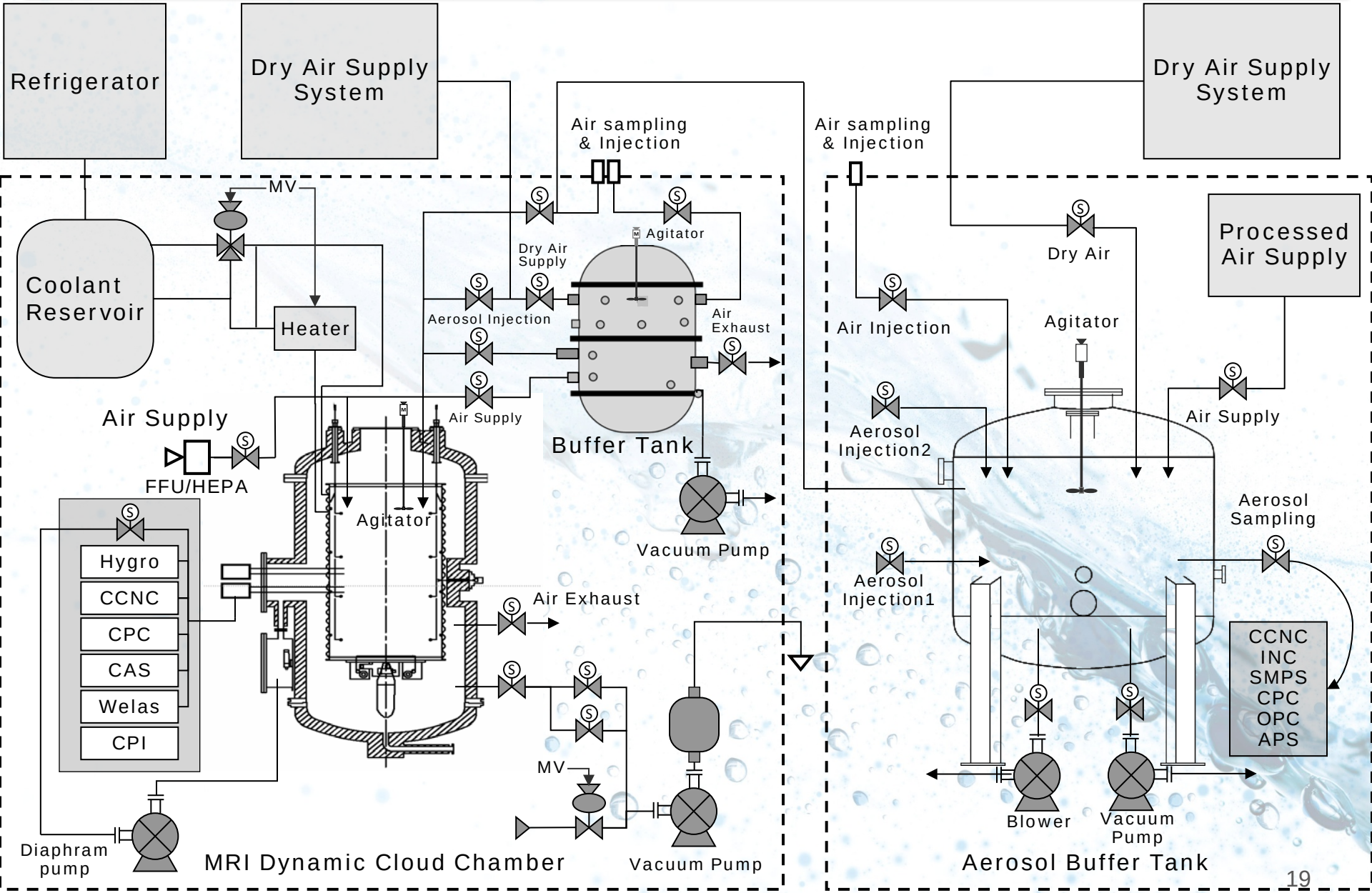

MRI dynamic cloud chamber exp.

Table 6. Exp. information

date	type	Conc. (#/cc)	ascent rate (m/s)	Tini	Tdini	TLCL	AFmax	Aave	INASmax
161117	Al_2O_3	1360	5	5	-13.3	-16.9	0.0043	1.6E-12	2.7E+09
161118	Al_2O_3	2940	5	5	-8.7	-11.5	0.0425	1.6E-12	2.6E+10
170106	Al_2O_3	1600	5	5	-6.5	-8.9	0.0205	1.6E-12	1.3E+10
170110	Fe_2O_3 #1	4200	5	5	-5.2	-7.5	0.0006	1.2E-12	4.9E+08
170111	Fe_2O_3 #1	8640	5	5	-10.5	-13.6	0.0014	1.2E-12	1.1E+09
170112	Fe_2O_3 #2	3580	5	-5	-13.9	-15.7	0.0031	3.9E-13	7.9E+09
170113	Fe_2O_3 #2	2880	5	-5	-11	-12.5	0.0042	3.9E-13	1.1E+10

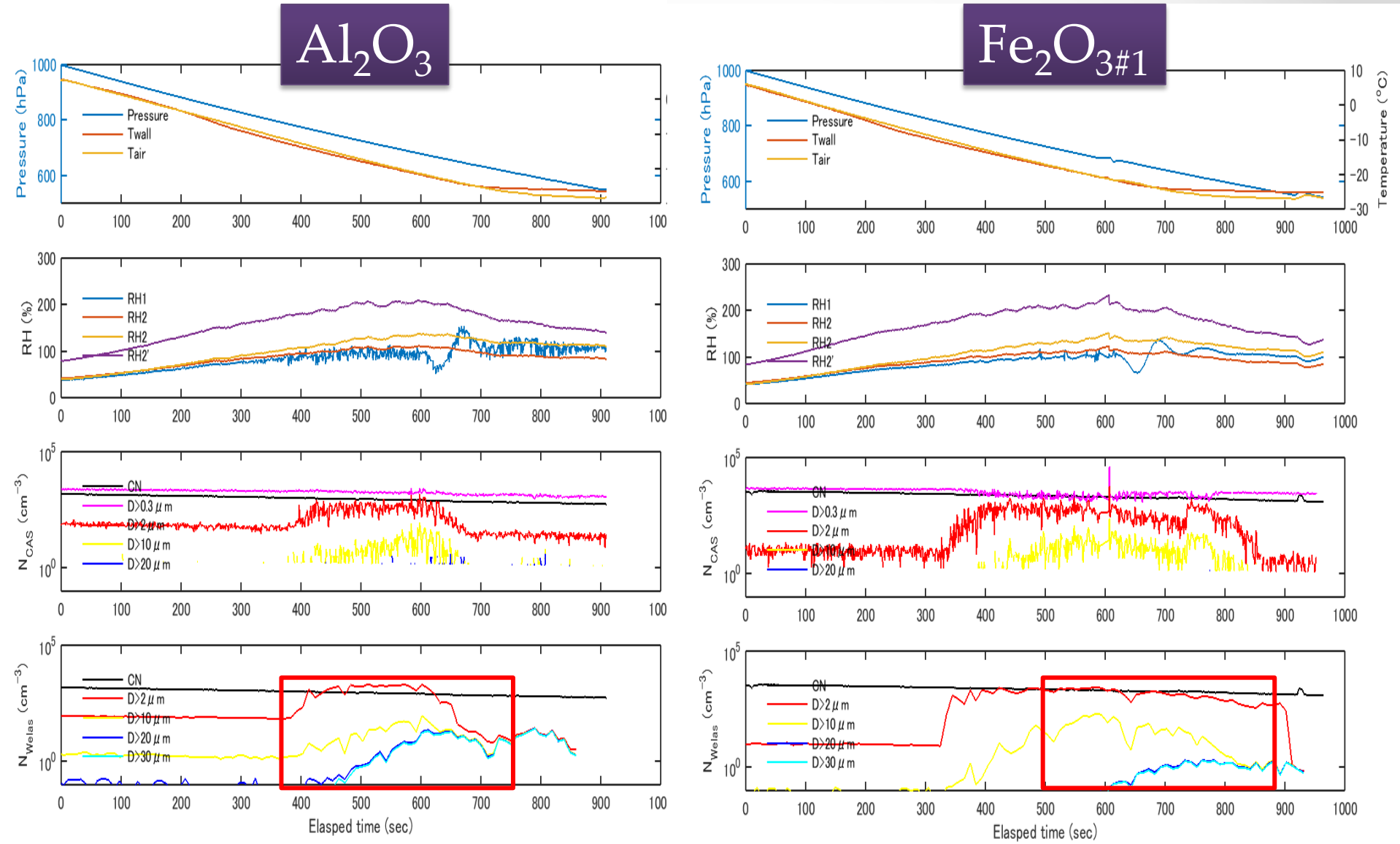

Fig 15. MRI dynamic chamber exp.

Activation fraction

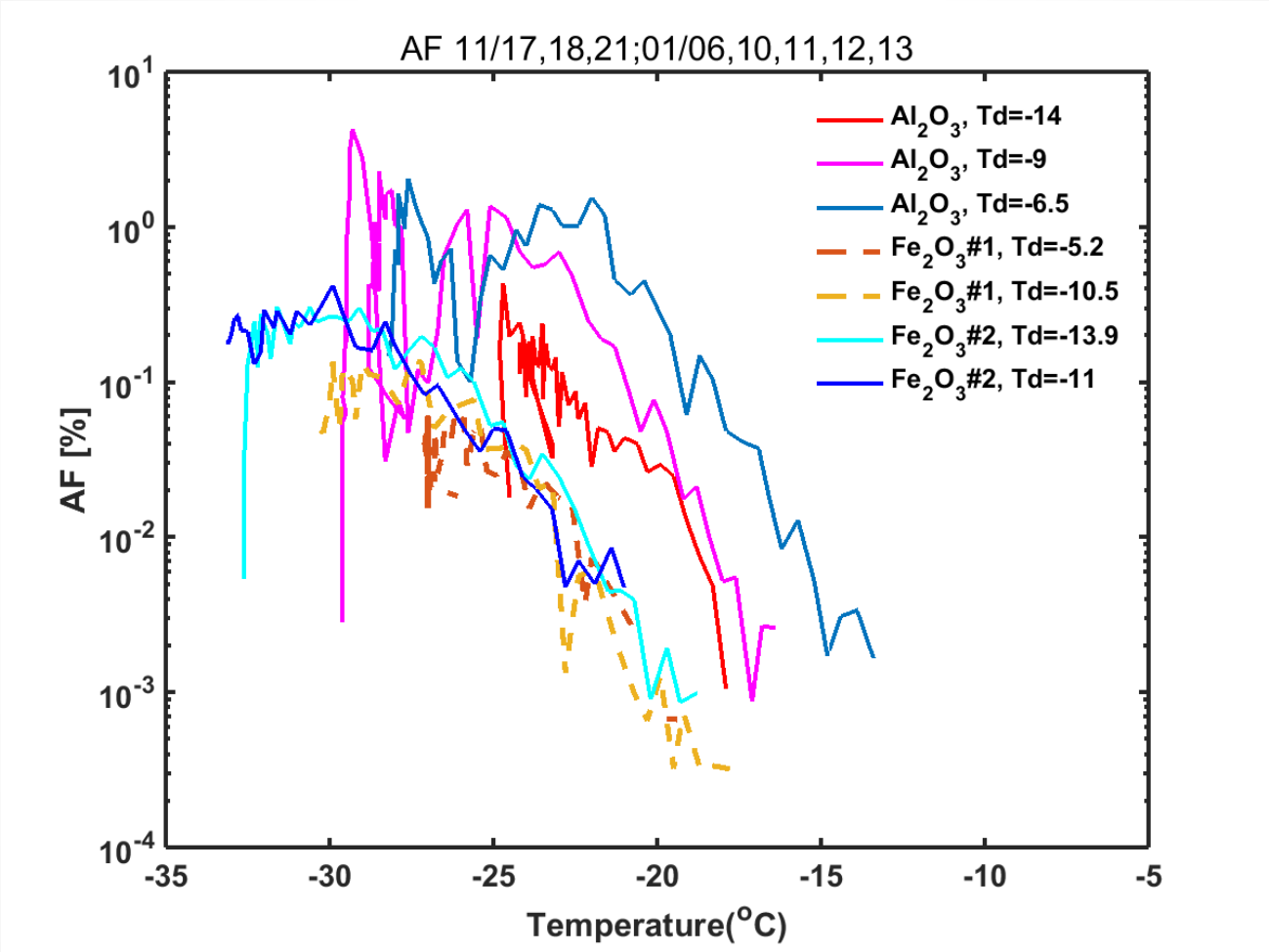

Fig 16. Activation fraction

INAS

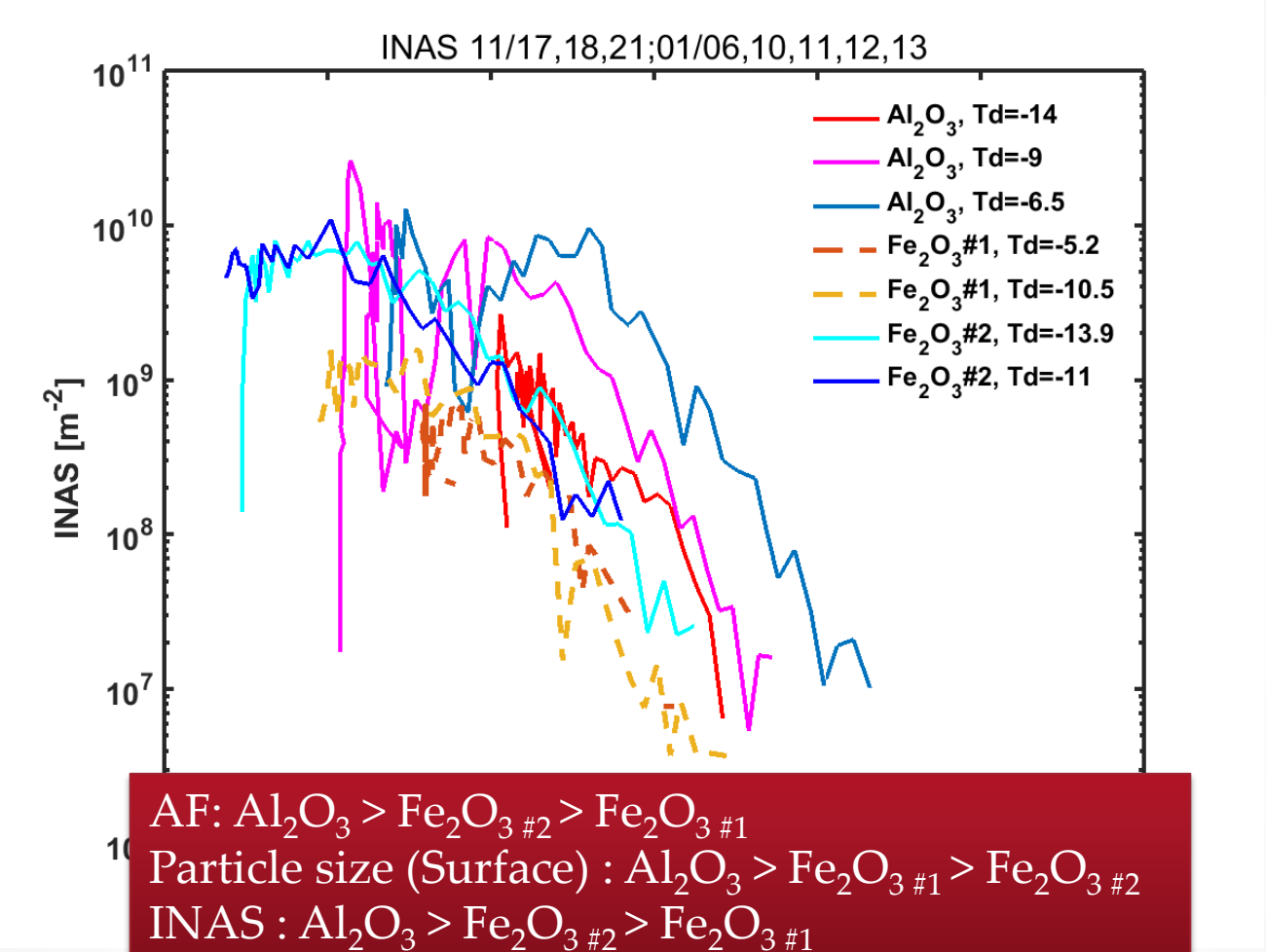

Fig 17. Results in INAS form

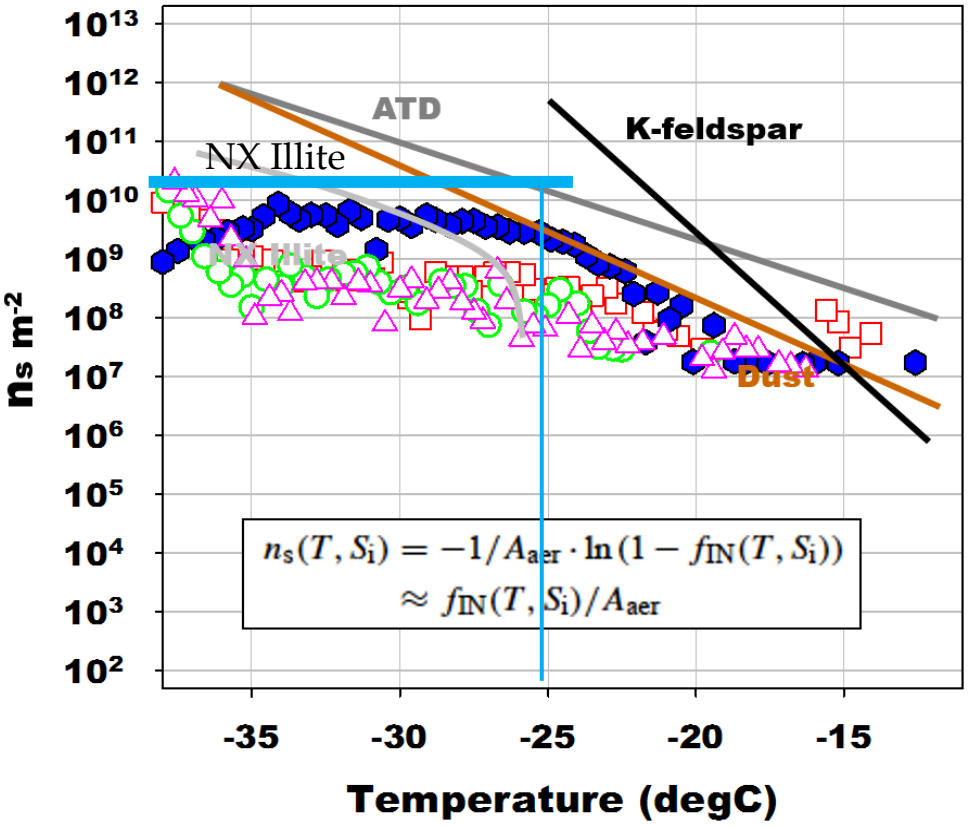

Niemand et al. 2012
Niemand et al. 2012
Atkinson et al. 2013
Broadly et al. 2012

Dust:
Asian dust (AD)
Saharan dust (SD)
Canary Island dust (CID)
Israel dust (ID)
Arizona test dust (ATD).

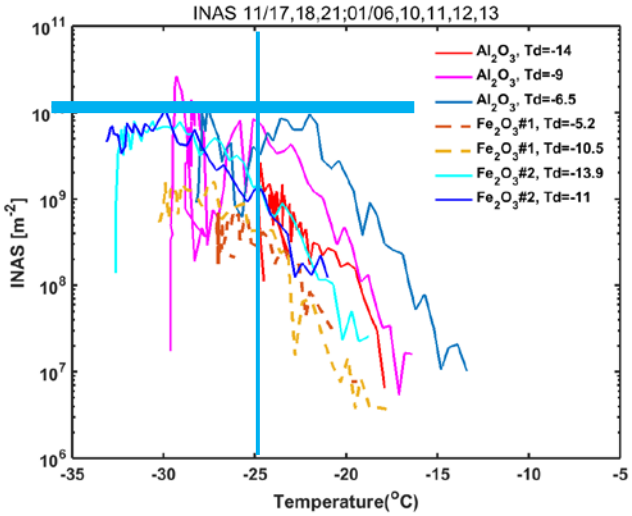

Fig 18. Previous results in INAS form

Previous study using MRI chamber

cellulose (セルロース)

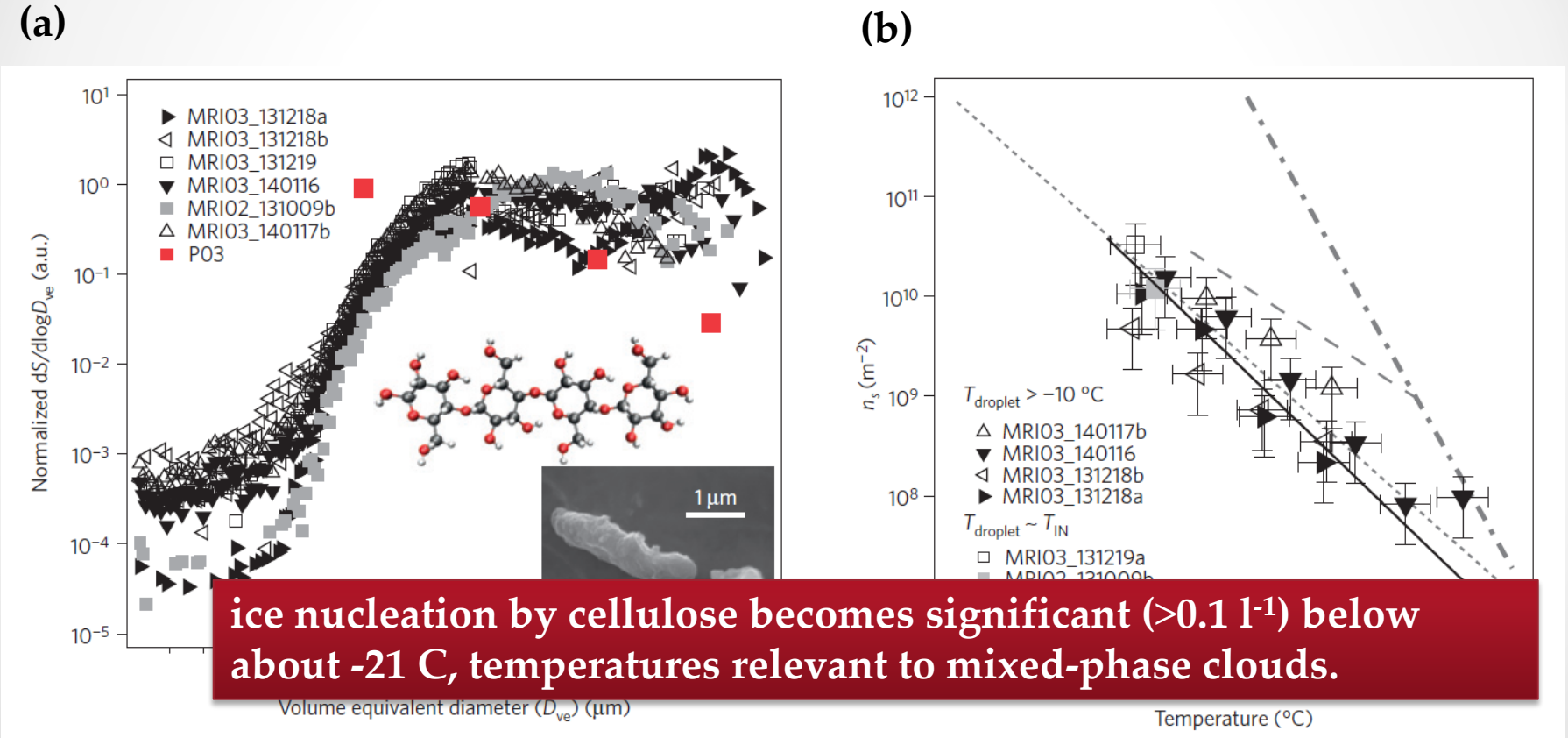

ice nucleation by cellulose becomes significant (>0.1 l^{-1}) below about -21 C, temperatures relevant to mixed-phase clouds.

Fig 19. (a) Size distribution of cellulose (b) Rsults in INAS form Hiranuma et al. (2015)

Discussion for cloud chamber exp.

- Coolant temperature issue (not low enough)
- Around -20℃, the ice crystal can be observed in cloud chamber exp.
- Which is the dominated mechanism, condensation or immersion freezing?
- Size issue, Al_2O_3 has broad size distribution inside the cloud chamber.
  - Size matters more than chemistry for cloud-nucleating ability (Dusek et al., 2006)
    - More particles are large than 0.2 μm of Al_2O_3

CFDC-type IN counter exp.

Table 7. Material information

type	Mean diameter	Aave
Al_2O_3	0.34	4.9E-13
Fe_2O_3 #1	0.35	4.8E-13
Fe_2O_3 #2	0.28	3.0E-13

Cut-off 1μm

IN measurement employed
Temperature:: -10 ~ -35 ℃
Relative humidity:
SSi ~ 0 % to SSw ~ +15 %

Fig 20. MRI IN Counter

CFDC-type IN counter exp.

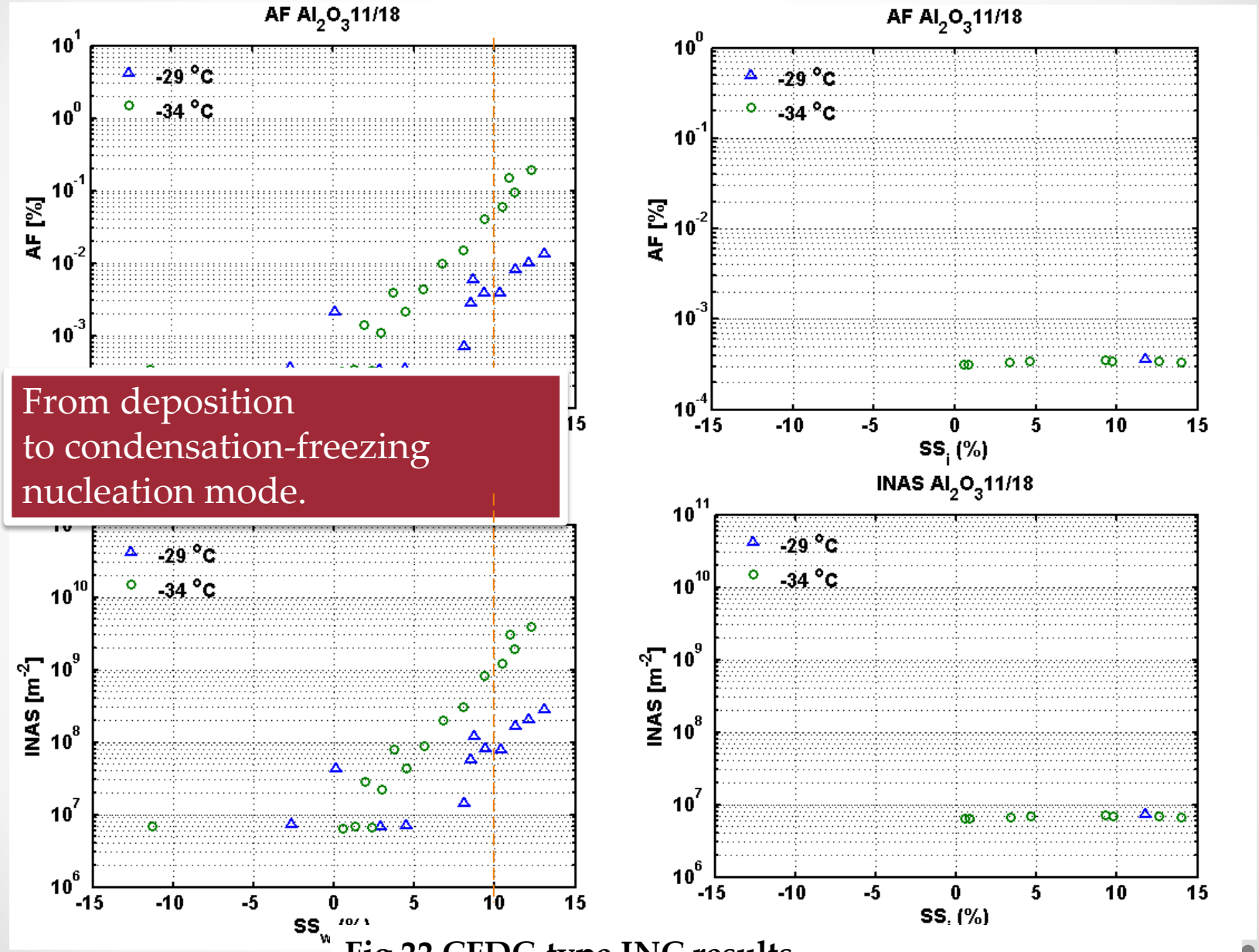

From deposition to condensation-freezing nucleation mode.

Fig.22 CFDC-type INC results

Discussion

- Is the metal oxide efficient enough as CCN/IN ?
  - Real atmospheric condition, particle size distribution
- How is the difference between laboratory and reality ?
  - Internal/external mixing
  - mixed-phase clouds
- Uncertainties during the experiment processes.
- We suggest a series of future studies investigating the ice nucleation activity of metal oxide in greater detail

Conclusion and ongoing work

- Kappa of three metal oxide particles are around 0.01-0.04
- Ice nucleation by two metal oxide becomes significant below about -20/-25 ℃, temperatures relevant to mixed-phase clouds.
- Al_2O_3 seems to have better IN ability than Fe_2O_3 both in cloud chamber exp. and CFDC-type INc exp.
  - Onset temperature is around -20℃ in cloud chamber exp.
  - Ability is like illite.
  - Onset temperature is around -30℃ in CFDC-type INc exp.

- Parcel model (Chen and Lamb,1994)– using kappa and INAS for parameterization (Yamashita et al., 2011, 2013; Hoose and Möhler, 2012)

...

Thanks for listening.